Plasmon-enhanced single photon source directly coupled to an optical fiber

Masakazu Sugawara,[1,2] Yining Xuan,[1,2] Yasuyoshi Mitsumori,[1,3] Keiichi Edamatsu,[1,*] and Mark Sadgrove[1,4,†]

[1]*RIEC, Tohoku University, Sendai 980-8577, Japan*

[2]*Department of Electronic Engineering, Graduate School of Engineering, Tohoku University, Sendai 980-8579, Japan*

[3]*Kitasato University, Sagamihara, Kanagawa 252-0373, Japan*

[4]*Tokyo University of Science, Shinjuku, Tokyo 162-8601, Japan*

(Received 29 April 2022; accepted 12 October 2022; published 29 November 2022)

A bright source of fiber-coupled, polarized single photons is an essential component of any realistic quantum network based on today's existing fiber infrastructure. Here, we develop a Purcell-enhanced, polarized source of single photons at room temperature by coupling single colloidal quantum dots to the localized surface plasmon-polariton modes of single gold nanorods, combined on the surface of an optical nanofiber. A maximum enhancement of the photon emission rate of 62 times was measured corresponding to a degree of polarization of 85%, and a brightness enhancement of four times in the fiber mode. Evanescent coupling of photons to the nanofiber guided modes ensures automatic coupling to a single mode fiber. Our technique opens the way to realizing bright sources of polarized single photons connected to fiber networks using a simple composite technique.

DOI: 10.1103/PhysRevResearch.4.043146

I. INTRODUCTION

The generation and storage of polarized single photons ("flying qubits") and their efficient coupling to existing fiber networks is an essential technology for the realization of quantum networks [1–4]. In addition, such photons should be generated at a high enough rate to keep pace with modern communication technologies in the gigahertz range. One research program which shows promise in achieving the above goals is the use of nanowaveguide-based cavities to produce waveguide coupled single photons with a Purcell-enhanced generation rate [5–10]. Nanowaveguide-based cavities are either automatically fiber coupled [11–15] or can be coupled to optical fibers with high efficiency [16].

The requirements for such schemes may be split into three main parts: (i) Efficient coupling of photons to the waveguide, (ii) enhancement of the rate of generated single photons, and (iii) enhancement of photon degree of polarization (DOP). Photonic-crystal-based nanowaveguide cavities are known to accomplish requirement (i) well, due to the overlap of the Purcell-enhanced cavity mode with the waveguide mode. However, with some notable exceptions [7], they achieve requirement (ii) to only a moderate degree, with enhancement factors of order 10 being common. More significantly, nanowaveguide-based cavities to date improve the degree of photon polarization only slightly, due to the mild cavity birefringence [12]. Nonetheless, photon polarization is essential for many photon-based quantum communication schemes and for schemes involving chiral quantum optical effects [17] suggesting that polarization enhancement is in vital need of attention.

The localized surface plasmon-polariton resonances (LSPRs) of metal nanostructures provide an important method of achieving polarization and brightness enhancement of single photon sources at room temperature. LSPRs function as Purcell regime resonators *par excellence* with rapid decay rates and large emitter-resonator coupling strengths [18–20]. In addition, they exhibit very large birefringence, with orthogonally polarized modes having resonance wavelengths separated by hundreds of nanometers. For an emitter with a sufficiently narrow bandwith, this fact allows selective enhancement of either the axial or transverse component of dipole emission for an emitter coupled to the LSPRs, resulting in a large increase in the degree of polarization of randomly polarized photon emitters. The use of metal nanostructure LSPRs on nanowaveguides offers an overlapping set of advantages compared with waveguide-based cavities [21]. Although (i) coupling to the waveguide mode is not in general enhanced (due to the approximate point dipole nature of typical LSPRs), (ii) brightness enhancement is relatively very large [22,23], and (iii) room-temperature polarization enhancement is unmatched [24–26]. It is therefore clear that one path to room-temperature, fiber-coupled polarized single photons requires a *combination* of waveguide-based cavities and LSPR-based emitter enhancement. However, demonstrations of LSPR-enhanced-and-polarized single photon emission on a nanowaveguide are lacking to date. Here, we developed an enhanced polarized single photon source at room temperature directly coupled to an optical fiber by depositing colloidal quantum dots (QDs) near single gold nanorods (GNRs) on the surface of an optical nanofiber.

*eda@riec.tohoku.ac.jp

†mark.sadgrove@rs.tus.ac.jp

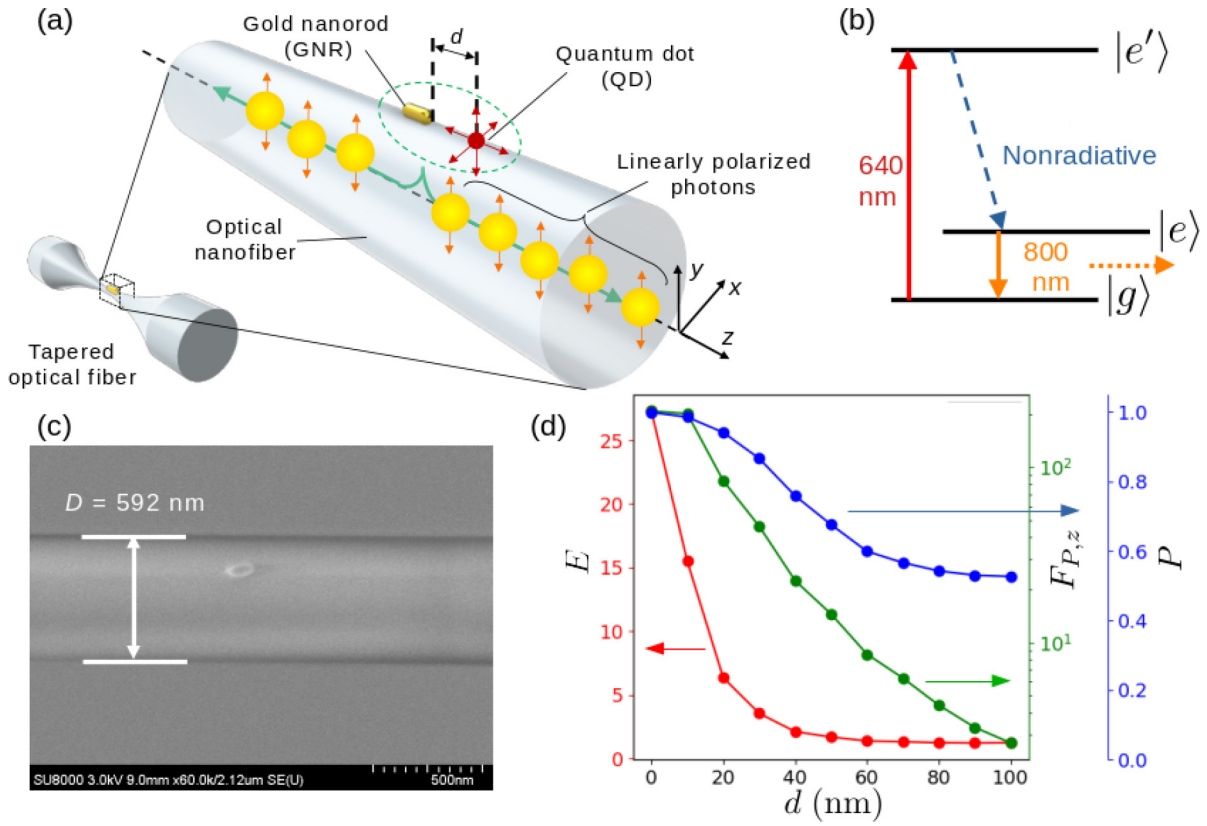

FIG. 1. Schematic illustration of the quantum-dot–gold-nanorod coupled system on an optical nanofiber. (a) Schematic illustration of the QD-GNR coupled system on an optical nanofiber. d is the separation between the edge of the gold nanorod (GNR) and the colloidal quantum dot (QD) nanocrystal. (b) Depiction of the relevant energy levels of the QD. (c) Image of the GNR taken using a scanning electron microscope (SEM). (d) Calculated intensity enhancement E, maximum Purcell enhancement factor $F_{P,z}$, and degree of polarization (DOP) P for photons propagating in the guided mode of the optical nanofiber as a function of d for a wavelength of 800 nm.

The spontaneous emission rate was enhanced due to the LSPR of the GNRs with enhancement factors of up to 62. Moreover, due to the strong polarization anisotropy of the plasmonic resonance of the GNRs, we also measured an increase in the DOP to 85% for photons emitted from the QD-GNR coupled system compared with a DOP of $\lesssim 50\%$ for QDs by themselves. Lastly, despite the fact that coupling efficiency to the fiber is not directly enhanced by this technique, a maximum enhancement of single photon intensity in the fiber modes of about 3.8 times was observed over the *entire* QD bandwidth. This is in contrast to cavity-based techniques, which typically only give strong enhancement for a small portion of the room-temperature QD bandwidth [12]. The above values were found to be in good agreement with simulation results.

We note from the outset that our present study should be seen as a proof of principle and an examination of the specific challenges for characterizing and utilizing LSPR-enhanced QDs coupled to an optical nanofiber. In this paper, the probabilistic nature of the deposition (as described below) of GNRs and QDs makes the technique difficult to scale up, but existing methods of accurate deposition can in principle be utilized with this method, solving this problem [22,27]. It is also pertinent to note from the beginning that plasmon-enhanced single photon emission can display reduced single photon purity [28] and, indeed, this is the case in our study also. Nonetheless, as will be seen below, our sources do show sufficiently good antibunching to be characterized as single photon sources, and thus the focus of the present research is on the large enhancement achievable by this method relative to previous nanofiber cavity techniques.

II. PHYSICAL PRINCIPLES AND EXPERIMENT

A schematic illustration of the experiment is shown in Fig. 1(a). The colloidal QD crystal emits single photons with a wavelength λ_{QD} and a spontaneous emission lifetime τ_1, and a portion of the emitted photons are coupled into the guided mode of the optical nanofiber. If we place a GNR near the QD and the enhancement spectrum of the LSPR corresponding to the rod axis overlaps with the emission spectrum of the QD, the spontaneous emission of the QD will be greatly enhanced due to the Purcell effect.

The QD is at room temperature and is excited by linearly polarized light far from resonance (nominal emission wavelength 800 nm, excitation wavelength 640 nm). In this case, as shown in Fig. 1(b), the excitation populates a higher excited state $|e'\rangle$ which decays nonradiatively through phononic processes (blue dashed arrow) very rapidly compared with the optical transition from $|e\rangle$ to $|g\rangle$ (orange arrow) which produces the single photons in this experiment. This excitation process is known to produce unpolarized photons in many

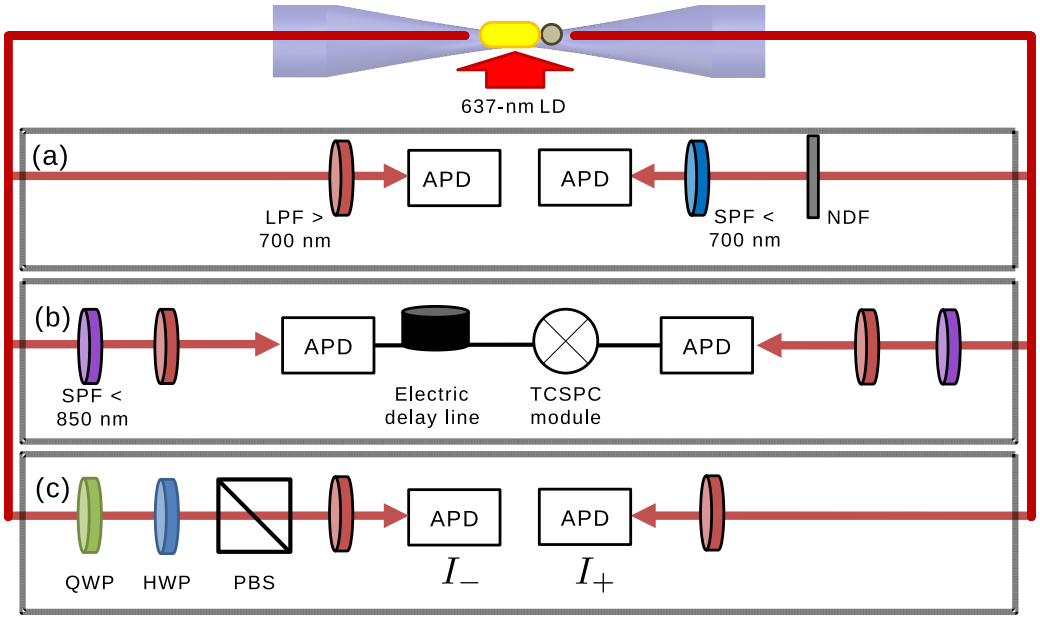

FIG. 2. Experimental setup. The filter configuration is shown for (a) the fiber scanning measurement, (b) the photon coincidence measurement, and (c) the photon polarization measurement. LD, laser diode; LPF, long-pass filter; APD, avalanche photodiode; SPF, short-pass filter; NDF, neutral-density filter; TCSPC, time-correlated single photon counting module; QWP, quarter-wave plate; HWP, half-wave plate; PBS, polarization beam splitter. We refer to the signals detected at the APDs on the right-hand side (left-hand side) as $I_+(I_-)$.

quantum emitters, and degrees of polarization of less than 25% in CdSe microcrystals [29] down to near zero in nitrogen vacancy (NV) centers [30] have been predicted and observed for reasons including the phonon-mediated decay process and the population of orbitals with different polarizations at room temperature.

However, because the LSPR in the wavelength range of the QD has a single polarization, spontaneous emission from the QD with a polarization lying along the GNR axis will be principally enhanced, leading to a large increase in the DOP of the emitted single photons [31–33]. A scanning electron microscope (SEM) image of a single gold nanorod located on the surface of a nanofiber is shown in Fig. 1(c). We calculated the expected values of the Purcell enhancement factor $F_{p,z}$ along with the DOP of the emitted photons P, and the intensity enhancement in the nanofiber guided modes E using the finite-difference time-domain (FDTD) method. The results are shown in Fig. 1(d). For the case where the QD comes into contact with the GNR ($d = 0$), $F_{p,z}$ is expected to exceed 200, and P approaches unity.

Note that we use a simple model for the system in which the QD is located along the rod axis. Due to the rapid decay of the evanescent electric field associated with the plasmonic resonance of the rod, coupling between the QD and the GNR falls by a factor of $1/e$ for an azimuthal angle difference of just 7° between the GNR and the QD. For this reason, in situations such as those considered in this paper where the Purcell enhancement is large, it is reasonable to assume that the QD and the GNR are aligned in this manner.

In experiments, we deposited nanorods (A12-50-800-CTAB-DIH-1-25, Nanopartz) on the surface of the optical nanofiber as described in Ref. [34]. After confirmation of a single GNR deposition [34,35], we touched a droplet of the solution containing the QDs to the nanofiber at the position of the observed scattering points of the GNRs leading to QD deposition. After particle deposition, photoluminescence (PL) from the QDs and scattered light from GNRs deposited on the optical nanofiber were measured using the experimental setup depicted in Fig. 2. The optical nanofiber was mounted on a three-axis computer-controllable translation stage. We excited the deposited particles with focused laser light (wavelength 637 nm) and detected PL from QDs or scattered light from GNRs using fiber-coupled avalanche photodiodes (APDs) after passing through the relevant filter system [Fig. 2(a)]. Photon correlation measurements were made using the setup shown in Fig. 2(b).

To measure P, we used the filter and polarizer configuration shown in Fig. 2(c). After rotating the state to the linear polarization basis using the quarter-wave plate (QWP), we measured the transmission through the half-wave plate (HWP) and polarization beam splitter (PBS) with respect to the angle of the HWP. The DOP lies between 0 and 1 and is found from the amplitude of a sinusoidal fit to these data.

The same setup shown in Fig. 2(c) is also used for measurements of the photon count rate, as used to calculate the enhancement factor E. In this case, we used measurements of the unfiltered photon count rate I_+, which is proportional to the intensity. We note that in our experiments, significant differences in the maximum count rate between the left- and right-hand sides of the fiber were never observed, and thus we assume that I_+ is half of the total photon count rate coupled to the nanofiber. E was estimated from these measurements by taking the ratio of the maximum intensity for the QD-GNR case to that for the QD-only case. As discussed below, for comparison we also calculate E by measuring the *average* photon count rate in both cases when the QD was in the "on" state (i.e., ignoring the periods where the QD does not emit due to blinking). Both methods agree within error.

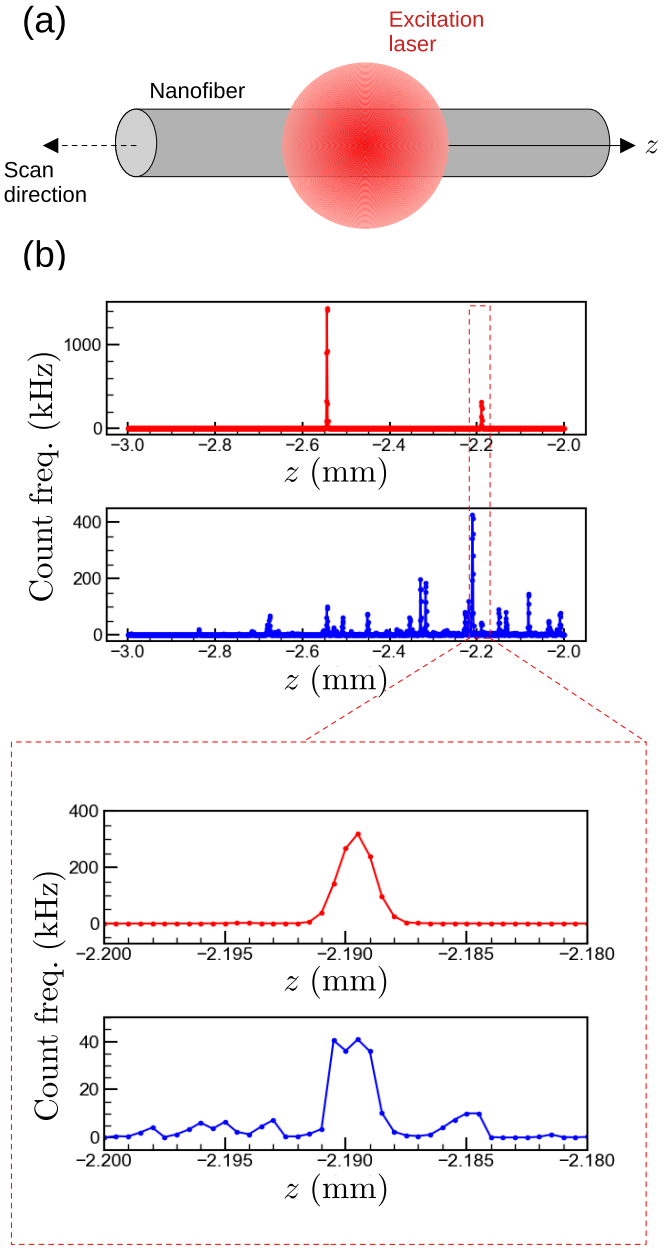

FIG. 3. Measurements for single gold rods and single QDs. (a) Schematic depiction of the sweep used to detect gold nanorods and QDs. (b) Results of a sweep showing detection of gold nanorods (red points, upper panel) and QDs (blue points, lower panel). The inset shows a zoomed-in image revealing that gold-rod and QD peaks are overlapped near $z = -2.19$. Here, freq., frequency.

III. RESULTS

We first measured the distribution of the deposited particles as depicted in Fig. 3(a). Results are shown in Fig. 3(b), with the PL (scattered) light signal displayed in the top (bottom) panel. Zooming in on the bright peak from the GNR around $z = -2.19$ mm [inset, Fig. 3(b)], the two peaks from the GNR and the QD deposition are seen to clearly overlap within the ∼5-μm spot size of the excitation laser, and thus the possibility of coupling between a GNR and a QD exists in this case. We now discuss measurements made for depositions where a QD and a GNR were found at the same position. First, we consider the second-order correlation function $g^{(2)}(\tau)$. Measurement of $g^{(2)}(\tau)$ provides two principal pieces of information about the coupled QD-GNR light source. First, a value $g^{(2)}(0) < 0.5$ indicates single-photon-dominant light emission. Second, the rise time T of $g^{(2)}(\tau)$ as $|\tau|$ increases gives the emitter lifetime. In particular, normalized photon coincidences from a single quantum emitter show antibunching given by

$$g^{(2)}(\tau) = 1 - \exp\left(-\frac{|\tau|}{T}\right), \tag{1}$$

where [27,36]

$$T = (\alpha P_{\text{exc}} + 1/\tau_1)^{-1}, \tag{2}$$

αP_{exc} is the power-dependent excitation rate, and τ_1 is the intrinsic decay time of the emitter. Coupling of a QD to a GNR gives rise to a decrease in T due to the Purcell effect, and thus the value of T relative to the uncoupled value T_0 gives information about the degree of fluorescence enhancement at a given excitation power.

Experimental measurements were made by correlating the PL signals taken from both ends of the optical fiber. Photon coincidences as a function of interval τ were recorded using a time-correlated single photon counting module (TCSPC; TimeHarp200, PicoQuant). Short-pass filters (SPFs) of 850 nm cutoff wavelength were inserted to reduce the effect of weak photon emission from the APDs themselves [37]. We first focus on measurements of $g^{(2)}(\tau)$ at a given excitation power. In particular, measurements of antibunching were made for excitation powers between 2 and 3 μW for the case of an uncoupled QD and for five different coupled QD-GNR samples. In this narrow power range, there is little power-induced variation of T, and differences reflect the strength of coupling between the QD and the GNR.

Figure 4(a) shows the case for an uncoupled QD on an optical nanofiber with an estimated diameter of 530 nm. Here, $g^{(2)}(0)$ was found to be 0.015 ± 0.002, and T was found to be 213 ± 1 ns, where the errors are one standard deviation calculated from the covariance of the fitted parameters. These values are in good agreement with typical values found in previous studies of single QDs on optical nanofibers [27]. Figure 4(b) shows a measurement of $g^{(2)}(\tau)$ for the QD-GNR sample which gave the largest overall enhancement in our experiments. The antibunching dip is seen to have a value $g^{(2)}(0) = 0.40 \pm 0.02$. Comparison of the results shown in Figs. 4(a) and 4(b) clearly reveals large Purcell enhancement, with T reduced to 3.1 ± 0.1 ns in Fig. 4(b).

Next, we consider measurements of the degree of polarization P of the fluorescence. Figure 4(c) shows a measurement of visibility made using the setup shown in Fig. 2(c) for the same uncoupled QD on a nanofiber measured in Fig. 4(a). The corresponding DOP was found to be $P = 0.40 \pm 0.01$. Figure 4(d) shows similar measurements made for the same sample measured in Fig. 4(b). We see an enhancement of the DOP in this case up to $P = 0.85 \pm 0.01$. These observations are consistent with Purcell enhancement by the highly anisotropic plasmon resonance of the gold nanorod. In addition, the orange points in Fig. 4(d) show the same polarization measurement applied to light from the nominally linearly

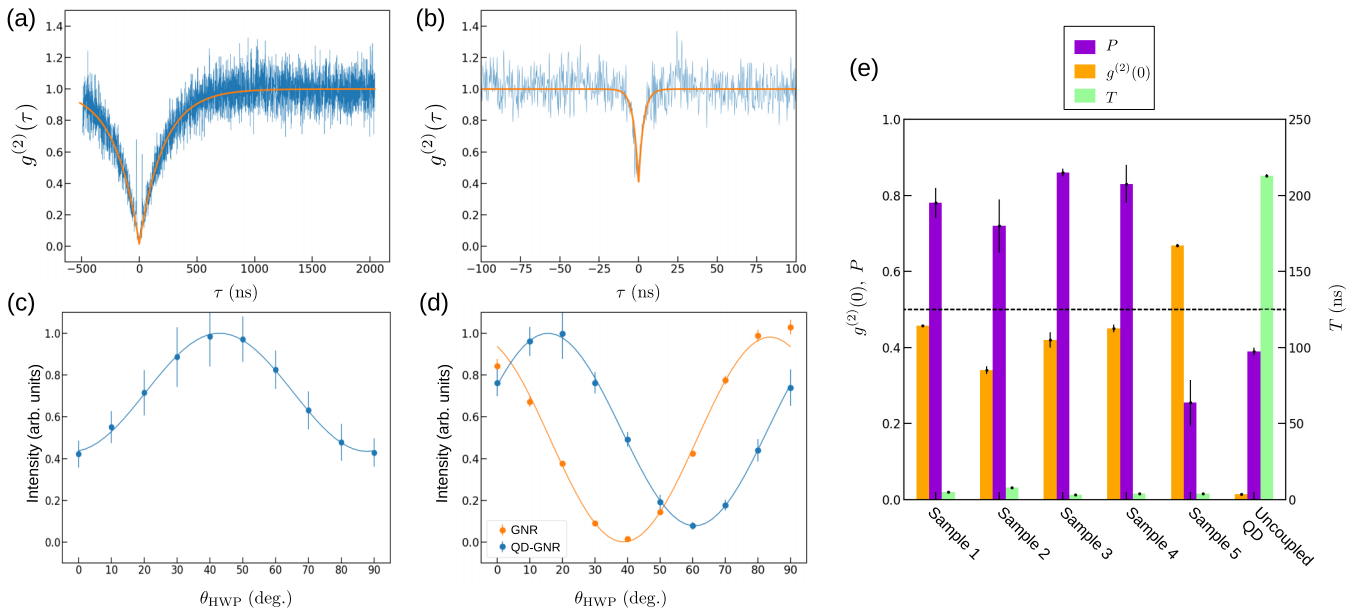

FIG. 4. (a) and (b) Intensity correlation $g^{(2)}(\tau)$ for the case of QDs uncoupled and coupled to a GNR, respectively. Solid orange lines show a fit of Eq. (1) to the data. (c) and (d) Measurements of the degree of polarization P for the cases shown in (a) and (b), respectively. Points with error bars show the measured values, with error bars showing the standard deviation over five separate measurements. Solid curves show a sinusoidal fit to the data. In (d), the points and orange curve show the degree-of-polarization measurement results for polarized light scattered from the gold nanorod into the fiber modes. (e) Summary showing $g^{(2)}(0)$ (orange bars), degree of polarization P (purple bars), and rise time T (green bars) for five different samples where coupling between a QD and a GNR was present. Sample 3 corresponds to the data shown in (b) and (d). The final set of bars shows the case for a single quantum dot without any coupling to a GNR and corresponds to the data shown in (a) and (c).

polarized excitation laser scattered by the gold nanorod directly into the nanofiber. This scattered light should preserve the pure polarization of the excitation laser light, leading to a perfect degree of polarization of 1. Indeed, the measured value of P in this case is 0.99 ± 0.02. This measurement acts as a double check on our polarization measurement system. In all cases, we note that the phase of the sinusoidal variation has no physical significance and is related to the unique path taken by the light through the fiber before detection for each specific particle.

We now comment briefly on the lower than expected value of the degree of polarization in the case of the QD alone. Although a QD emitting into free space is expected to have a random polarization ($P = 0$), the different boundary conditions for dipole orientations normal and tangential to the fiber surface lead to differences in the Purcell factor and the coupling efficiency of the dipole emission into the fiber. In particular, the Purcell factor for the normally oriented dipole is 1.5, whereas that for a tangential dipole is 1, i.e., no Purcell effect is present in the tangential case. This anisotropy gives rise to a degree of polarization which is ideally as high as 0.5. Nonetheless, the value of 0.5 is obtained numerically for an ideal fiber, i.e., for a fiber with a perfectly smooth surface. Although the exact reason for the lower than expected DOP is still under investigation, it seems plausible that it may be related to surface roughness and scattering which reduce the Purcell effect for the normally oriented dipole moment leading to a reduction in the degree of polarization compared with the ideal case.

Finally, we summarize the results for five samples (samples 1–5) in which a QD was found to be deposited close to a GNR on a nanofiber and compare the results with an uncoupled QD as shown in the bar chart in Fig. 4(e). The results indicate coupling between a QD and a GNR according to the greatly reduced values of T compared with the uncoupled-QD case. Note that sample 3 corresponds to the measurements shown in Figs. 4(b) and 4(d) and was the sample for which the smallest value of T and the largest value of P were measured. The lowest antibunching dip was seen for sample 2 with $g^{(2)}(0) = 0.34 \pm 0.01$, clearly in the regime of single-photon-dominant emission. It is interesting to note that the only sample, sample 5, for which $g^{(2)}(0)$ was clearly larger than 0.5 (indicating that two or more QDs were contributing strongly to the fluorescence) also showed a decreased value of P, in comparison to the other samples, where P was found to be enhanced relative to the uncoupled case. The relatively small value of P in this case suggests that only one of the two QDs in sample 5 was significantly coupled to the GNR.

To measure the maximum Purcell factor produced by our technique, we measured T at various excitation powers for both the uncoupled QD measured above and sample 3, where the best coupling was observed. Note that the power at which saturation of the QD intensity was observed for the QD-GNR system was about 3 μW. The saturation behavior of these QDs for varying excitation power has been studied in detail in Ref. [27]. Figure 5(a) shows the power dependence of T in the case of a QD uncoupled to a GNR (blue circles) and for sample 3 (yellow stars). By fitting the experimental data using Eq. (2), we evaluated the spontaneous emission lifetimes of the single QD and the QD-GNR coupled system as $\tau_0 = \tau_1^{\mathrm{QD}} = 280$ ns and $\tau_1^{\mathrm{QD\text{-}GNR}} = 4.5$ ns, respectively.

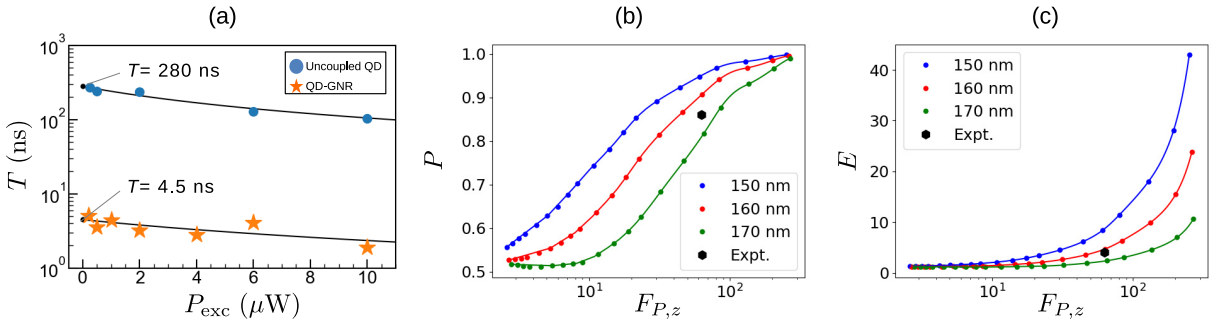

FIG. 5. Evaluation of the peak Purcell factor. (a) Measurements of rise time T as a function of excitation power for the case of a single QD uncoupled to a GNR (blue circles) and a QD coupled to a GNR (yellow stars). Solid lines show a fit to the data using Eq. (2). (b) Simulation results (discrete points) showing the polarization P vs the peak Purcell factor $F_{P,z}$ for the nanorod lengths indicated in the legend. The experimentally measured value is shown by a black hexagon. (c) Simulation results (discrete points) showing the intensity enhancement E vs the peak Purcell factor $F_{P,z}$ for the nanorod lengths indicated in the legend. The experimentally measured value is shown by a black hexagon. In (b) and (c), curves connecting the points are splines fitted to guide the eye.

Therefore the Purcell enhancement factor can be estimated to be $\tau_0/\tau_1^{\text{QD-GNR}} = 62$. Note that this estimate of the Purcell factor relies on the measured value of τ_0 being representative of the entire QD ensemble. Thorough studies of the distribution of τ_0 for the same QDs coupled to optical nanofibers have been performed in previous work [27], allowing us to assign an uncertainty to τ_1^{QD} of 30%. Using this value, a rough estimate of the uncertainty of the Purcell enhancement factor measured here was found to be $F_{P,z} = 62 \pm 26$.

We also made measurements of the maximum photon count rate achieved in the case of the uncoupled QD and sample 3. These rates were found to be 35.7 and 135.9 kHz in the case of uncoupled-QD and GNR-QD systems, respectively. Thus the enhancement of fluorescence coupled to the fiber modes *over the entire QD bandwidth* was found to be $E = 3.8$.

We note that corresponding average count rates achieved for the same samples were found to be 25 ± 4 and 85 ± 16 kHz, respectively. The ratio of the averages gives an alternative value of $E = 3.4 \pm 0.8$, which includes the value found by taking the ratio of maxima within experimental error. The large standard deviation of the results is mostly due to blinking of the QDs.

IV. DISCUSSION AND CONCLUSION

Measurement of the maximum Purcell factor as shown in Fig. 5(a) allows us to make a detailed comparison of the results with predictions based on the FDTD method. We calculated the degree of polarization P, intensity enhancement E, and maximum Purcell factor $F_{P,z}$ for a number of separations d between the QD and the GNR. Note that both P and E are averages over the probability distribution defined by the normalized QD spectrum [center wavelength 760 nm, full width at half maximum (FWHM) 50 nm to match the case of sample 3]. Although the GNRs used in our experiment had a nominal length of 160 nm, in reality a spread in values of about 10% is present in the sample, and the scanning electron microscope measurements are at the same level of accuracy. For this reason, we also performed simulations for the cases where the GNR length was 150 and 170 nm for comparison. For simplicity we oriented the GNR along the z axis. Simulation results for P vs $F_{P,z}$ and E vs $F_{P,z}$ are shown in Figs. 5(b) and 5(c), respectively, with symbols as indicated in the legend. The experimental value for sample 3 is shown as a black hexagon in both cases. We see good agreement between the measured values and the simulation-predicted values for the nominal rod length of $L = 160$ nm.

On the other hand, the occurrence of relatively large values of $g^{(2)}(0) \lesssim 0.5$ for the coupled QD-GNR systems measured here is a curious feature which may be explained by more detailed theoretical treatments in the future. The increase in $g^{(2)}(0)$ for QDs coupled to the localized plasmon resonances of metal nanoparticles has been noted elsewhere [28] and has been partly explained theoretically as fluorescence from the nanoparticle itself during the periods where the quantum dot is excited [38]. It is possible that $g^{(2)}(0)$ might be improved by adjusting the excitation wavelength or polarization, although this is beyond the scope of the present study.

It is also interesting to speculate on how other aspects of single photon generation might be affected by the scheme presented above. Perhaps most interesting is the question of indistinguishability of photons, and how this might be improved for quantum dots coupled to GNRs. On the one hand, the increased degree of polarization clearly increases photon indistinguishability. On the other hand, the broadness of the LSPR resonance relative to the narrow resonances achieved with photonic crystal cavities means that photons will in general be distinguishable in the frequency domain using this method, due to the large emission bandwidth of the QDs. This suggests that the best path forward for applications involves the use of plasmonically enhanced QDs used together with on-fiber cavities.

In conclusion, we have developed a polarized rate-enhanced single photon source coupled to an optical fiber at room temperature by using coupling between QD nanocrystals and the LSPRs of anisotropic gold nanoparticles. The use of chiral gold nanoparticles in place of gold nanorods may allow the realization of circularly polarized photons, and thus chiral quantum optics effects at room temperature [39]. The system is also a promising platform for quantum plasmonics research, due to the convenience of the nanofiber substrate, which also doubles as a collection device for emitted photons.

Note added. We recently became aware of a similar study to the one reported here [40].

ACKNOWLEDGMENTS

This research was partially supported by MEXT Quantum Leap Flagship Program (MEXT Q-LEAP) Grant No. JPMXS0118067581 and JSPS KAKENHI Grant No. JP20H01831. M. Sadgrove acknowledges support from the Nano-Quantum Information Research Division of Tokyo University of Science and a JSPS KAKENHI Grant-in-Aid for Transformative Research Areas (Grant No. JP22H051351). This research was partially performed using the facilities of the Fundamental Technology Center, Research Institute of Electrical Communication, Tohoku University.

[1] H. J. Kimble, The quantum internet, Nature (London) **453**, 1023 (2008).

[2] C. Y. Lu and J. W. Pan, Quantum-dot single-photon sources for the quantum internet, Nat. Nanotechnol. **16**, 1294 (2021).

[3] R. Uppu, L. Midolo, X. Zhou, J. Carolan, and P. Lodahl, Quantum-dot-based deterministic photon-emitter interfaces for scalable photonic quantum technology, Nat. Nanotechnol. **16**, 1308 (2021).

[4] M. Brekenfeld, D. Niemietz, J. D. Christesen, and G. Rempe, A quantum network node with crossed optical fibre cavities, Nat. Phys. **16**, 647 (2020).

[5] K. Okamoto, I. Niki, A. Shvartser, Y. Narukawa, T. Mukai, and A. Scherer, Surface-plasmon-enhanced light emitters based on InGaN quantum wells, Nat. Mater. **3**, 601 (2004).

[6] H. Iwase, D. Englund, and J. Vučković, Analysis of the Purcell effect in photonic and plasmonic crystals with losses, Opt. Express **18**, 16546 (2010).

[7] L. Li, T. Schröder, E. H. Chen, M. Walsh, I. Bayn, J. Goldstein, O. Gaathon, M. E. Trusheim, M. Lu, J. Mower, M. Cotlet, M. L. Markham, D. J. Twitchen, and D. Englund, Coherent spin control of a nanocavity-enhanced qubit in diamond, Nat. Commun. **6**, 6173 (2015).

[8] I. Aharonovich, D. Englund, and M. Toth, Solid-state single-photon emitters, Nat. Photonics **10**, 631 (2016).

[9] T. Schröder, S. L. Mouradian, J. Zheng, M. E. Trusheim, M. Walsh, E. H. Chen, L. Li, I. Bayn, and D. Englund, Quantum nanophotonics in diamond, J. Opt. Soc. Am. B **33**, B65 (2016).

[10] F. Liu, A. J. Brash, J. O'Hara, L. M. P. P. Martins, C. L. Phillips, R. J. Coles, B. Royall, E. Clarke, C. Bentham, N. Prtljaga, I. E. Itskevich, L. R. Wilson, M. S. Skolnick, and A. M. Fox, High Purcell factor generation of indistinguishable on-chip single photons, Nat. Nanotechnol. **13**, 835 (2018).

[11] K. P. Nayak, P. Zhang, and K. Hakuta, Optical nanofiber-based photonic crystal cavity, Opt. Lett. **39**, 232 (2014).

[12] R. Yalla, M. Sadgrove, K. P. Nayak, and K. Hakuta, Cavity Quantum Electrodynamics on a Nanofiber Using a Composite Photonic Crystal Cavity, Phys. Rev. Lett. **113**, 143601 (2014).

[13] A. W. Schell, H. Takashima, S. Kamioka, Y. Oe, M. Fujiwara, O. Benson, and S. Takeuchi, Highly efficient coupling of nanolight emitters to a ultra-wide tunable nanofibre cavity, Sci. Rep. **5**, 9619 (2015).

[14] W. Li, J. Du, and S. Nic Chormaic, Optical nanofiber-based cavity induced by periodic air-nanohole arrays, Appl. Phys. Lett. **110**, 253102 (2017).

[15] K. P. Nayak, M. Sadgrove, R. Yalla, F. Le Kien, and K. Hakuta, Nanofiber quantum photonics, J. Opt. **20**, 073001 (2018).

[16] T. G. Tiecke, K. P. Nayak, J. D. Thompson, T. Peyronel, N. P. de Leon, V. Vuletić, and M. D. Lukin, Efficient fiber-optical interface for nanophotonic devices, Optica **2**, 70 (2015).

[17] P. Lodahl, S. Mahmoodian, S. Stobbe, A. Rauschenbeutel, P. Schneeweiss, J. Volz, H. Pichler, and P. Zoller, Chiral quantum optics, Nature (London) **541**, 473 (2018).

[18] M. S. Tame, K. R. McEnery, Ş. K. Özdemir, J. Lee, S. A. Maier, and M. S. Kim, Quantum plasmonics, Nat. Photonics **9**, 329 (2013).

[19] S. I. Bozhevolnyi and J. B. Khurgin, The case for quantum plasmonics, Nat. Photonics **11**, 398 (2017).

[20] S. I. Bogdanov, A. Boltasseva, and V. M. Shalaev, Overcoming quantum decoherence with plasmonics, Science **364**, 532 (2019).

[21] A. Barreda, L. Mercadé, M. Zapata-Herrera, J. Aizpurua, and A. Martínez, Hybrid Photonic-Plasmonic Cavity Design for Very Large Purcell Factors at Telecommunication Wavelengths, Phys. Rev. Appl. **18**, 044066 (2022).

[22] S. Schietinger, M. Barth, T. Aichele, and O. Benson, Plasmon-enhanced single photon emission from a nanoassembled metal-diamond hybrid structure at room temperature, Nano Lett. **9**, 1694 (2009).

[23] C. T. Yuan, P. Yu, H. C. Ko, J. Huang, and J. Tang, Antibunching single-photon emission and blinking suppression of CdSe/ZnS quantum dots, ACS Nano **3**, 3051 (2009).

[24] D. C. Unitt, A. J. Bennett, P. Atkinson, D. A. Ritchie, and A. J. Shields, Polarization control of quantum dot single-photon sources via a dipole-dependent Purcell effect, Phys. Rev. B **72**, 033318 (2005).

[25] V. I. Kukushkin, I. M. Mukhametzhanov, I. V. Kukushkin, V. D. Kulakovskii, I. V. Sedova, S. V. Sorokin, A. A. Toropov, S. V. Ivanov, and A. S. Sobolev, Control of semiconductor quantum dot emission intensity and polarization by metal nanoantennas, Phys. Rev. B **90**, 235313 (2014).

[26] J. J. Cadusch, E. Panchenko, N. Kirkwood, T. D. James, B. C. Gibson, K. J. Webb, P. Mulvaney, and A. Roberts, Emission enhancement and polarization of semiconductor quantum dots with nanoimprinted plasmonic cavities: Towards scalable fabrication of plasmon-exciton displays, Nanoscale **7**, 13816 (2015).

[27] R. Yalla, K. P. Nayak, and K. Hakuta, Fluorescence photon measurements from single quantum dots on an optical nanofiber, Opt. Express **20**, 2932 (2012).

[28] T. B. Hoang, G. M. Akselrod, and M. H. Mikkelsen, Ultrafast room-temperature single photon emission from quantum dots coupled to plasmonic nanocavities, Nano Lett. **16**, 270 (2016).

[29] Al. L. Efros, Luminescence polarization of CdSe microcrystals, Phys. Rev. B **46**, 7448 (1992).

[30] N. Abe, Y. Mitsumori, M. Sadgrove, and K. Edamatsu, Dynamically unpolarized single-photon source in diamond with intrinsic randomness, Sci. Rep. **7**, 46722 (2017).

[31] C. Sonnichsen, T. Franzl, T. Wilk, G. vonPlessen, J. Feldmann, O. Wilson, and P. Mulvaney, Drastic Reduction of Plasmon

Damping in Gold Nanorods, Phys. Rev. Lett. **88**, 077402 (2002).

[32] T. Ming, L. Zhao, Z. Yang, H. Chen, L. Sun, J. Wang, and C. Yan, Strong polarization dependence of plasmon-enhanced fluorescence on single gold nanorods, Nano Lett. **9**, 3896 (2009).

[33] M. Joos, C. Ding, V. Loo, G. Blanquer, E. Giacobino, A. Bramati, V. Krachmalnicoff, and Q. Glorieux, Polarization Control of Linear Dipole Radiation Using an Optical Nanofiber, Phys. Rev. Appl. **9**, 064035 (2018).

[34] M. Sugawara, Y. Mitsumori, K. Edamatsu, and M. Sadgrove, Optical detection of nano-particle characteristics using coupling to a nano-waveguide, Opt. Express **28**, 18938 (2020).

[35] M. Sadgrove, M. Sugawara, Y. Mitsumori, and K. Edamatsu, Polarization response and scaling law of chirality for a nanofibre optical interface, Sci. Rep. **7**, 17085 (2017).

[36] A. V. Akimov, A. Mukherjee, C. L. Yu, D. E. Chang, A. S. Zibrov, P. R. Hemmer, H. Park, and M. D. Lukin, Generation of single optical plasmons in metallic nanowires coupled to quantum dots, Nature (London) **450**, 402 (2007).

[37] T. Huang, J. Shao, X. Wang, L. Xiao, and S. Jia, Photon emission characteristics of avalanche photodiodes, Opt. Eng. **44**, 074001 (2005).

[38] E. Waks and D. Sridharan, Cavity QED treatment of interactions between a metal nanoparticle and a dipole emitter, Phys. Rev. A **82**, 043845 (2010).

[39] H. E. Lee, H. Y. Ahn, J. Mun, Y. Y. Lee, M. Kim, N. H. Cho, K. Chang, W. S. Kim, J. Rho, and K. T. Nam, Amino-acid- and peptide-directed synthesis of chiral plasmonic gold nanoparticles, Nature (London) **556**, 360 (2018).

[40] K. M. Shafi, R. Yalla, and K. P. Nayak, Bright and polarized fiber in-line single photon source based on plasmon-enhanced emission into nanofiber guided modes, arXiv:2206.13029 [quant-ph].